Int. J. Appl. Ceram. Technol., 12 [S1] E82–E89 (2015)
DOI:10.1111/ijac.12260

Ferroelectric–Ferromagnetic Ceramic Composites Based on PZT with Added Ferrite

Przemysław Niemiec* and Dariusz Bochenek

Department of Materials Science, University of Silesia, 2, Śnieżna St., Sosnowiec 41–200, Poland

Artur Chrobak

Institute of Physics, University of Silesia, 4, Uniwersytecka St., Katowice 40–007, Poland

Piotr Guzdek

Institute of Electron Technology Cracow Division, 39, Zabłocie St, Cracow 30–701, Poland

Artur Błachowski

Institute of Physics, Pedagogical University of Cracow, 2, Podchorążych St., Cracow 30–084, Poland

The study presents a ferroelectric–ferromagnetic composite based on a doped PZT-type and ferrite powders. Ferroelectric powder (in amount of 90 wt-%) was based on multicomponent PZT-type materials, while nickel–zinc ferrite $Ni_{1-x}Zn_xFe_2O_4$ (in amount of 10 wt-%) served as the magnetic component of the composite. The syntheses of the ferroelectric–ferromagnetic composite's components were performed using solid-phase sintering, while final densification of the synthesized powder was achieved using free sintering. X-ray analysis of the composite confirmed the presence of strong maxima originating from particular PZT-type material phases, as well as weak peaks from the $Ni_{0.64}Zn_{0.36}Fe_2O_4$ ferrite, without foreign phases. The microstructure of the fracture of the ferroelectric–ferromagnetic composites shows that the ferrite grains on the surface of the ferroelectric component are distributed heterogeneously. Magnetic studies have characterized composite as a soft ferromagnetic material. The study indicated the influence of the magnetic subsystem on the electrical properties. In the two-phase PBZTMC–NZF ceramic composite, the magnetic component causes the decrease in electric permittivity and increased value of the dielectric losses.

Introduction

Multiferroics are a type of ferroic materials which have, simultaneously, at least two spontaneously ordered subsystems among the following states: ferromagnetic, ferroelectric, ferroelastic, or ferrotoroidic.[1,2] In multiferroic materials, the coupling interaction between the different order parameters could produce new effects, such as magnetoelectric ME effect.[3,4] The application capabilities of multiferroics depend mainly on the degree of coupling between specific subsystems (magnetic, electric, or elastic). An alternative to the multiferroic materials is multiferroic ceramic composites. For example, ferroelectro–ferromagnetic composites are a combination of materials with ferroelectric (piezoelectric) and ferromagnetic properties.[5,6] Electric and mechanical properties, together with the degree of electric and magnetic subsystems' coupling in these composites, are mainly related to the properties and percentage of each component of the composite. Depending on the chemical composition, crystal structure, temperature, etc., full coupling, semi-coupling, or lack of coupling of subsystems in multiferroics can occur.[2] The coupling of particular subsystems has been and continues to be the basic research problem concerning materials with multiferroic properties.[7]

The unique properties of ferroics and multiferroics have wide application in various fields of science.[8–12] They are used to build memory chips thanks to the hysteresis behavior of their ordering parameters, both on the basis of ferromagnetics and ferroelectrics. These types of modern memory chips would make it possible to save data in the form of ferroelectric signals, as well as to read the data in the form of a magnetic field.[1,4]

The aim of this work was to obtain a two-phase ferroelectric–ferromagnetic ceramic composite on the basis of a multicomponent ferroelectric PZT-type powder and ferromagnetic powder (nickel–zinc ferrite). The study presents the effect of combining ferroelectric and ferromagnetic material in the form of composite on the

*przemyslaw.niemiec@us.edu.pl

microstructure and the basic dielectric and magnetic properties.

Experimental Procedure

To obtain a ferroelectric–ferromagnetic composite (PBZTMC–NZF), synthesized ferroelectric PZT-type ceramic powder of $(Pb_{0.94}Ba_{0.06})(Zr_{0.52}Ti_{0.48})O_3$ + 0.1wt-% MnO_2 + 0.15wt-% Cr_2O_3 (PBZTMC), chemical composition, and nickel–zinc $Ni_{0.64}Zn_{0.36}Fe_2O_4$ (NZF) ferrite powder with ferromagnetic properties were used. The PBZTMC–NZF composite consisted of 90 wt-% of PZT-type ceramic powder and 10 wt-% of ferrite powder. The PZT-type ferroelectric powder was obtained using classic ceramic technology from PbO, ZrO_2, TiO_2, MnO_2, Cr_2O_3 oxides and $BaCO_3$ carbonate. Ferrite NZF was synthesized at 1000°C for 4 h (calcination method). The constituent powder's mixture of the composite PBZTMC was synthesized (compacting method) at a temperature of T_{synth} = 1050°C for t_{synth} = 4 h. The mixture of components PBZTMC–NZF was prepared using solid reaction synthesis (compacting method) under these conditions: T_{synth} = 850°C and t_{synth} = 2 h. The synthesized composite powders were densified (sintered) using the compacting free sintering method under these conditions: T_s = 1250°C for t_s = 2 h. Electrodes were applied to the composite specimen surfaces using the silver paste burning method for electrical tests. The technology for receiving composite specimens has been described in detail elsewhere.[5]

The X-ray measurements of the crystal structure were taken with a Phillips diffractometer (Almelo, the Netherlands), while the specimen fractures were examined with an SEM scanning microscope with field emission, HITACHI S-4700 (Tokyo, Japan), and with the energy-dispersive X-ray spectroscopy (EDS) Noran Vantage and EPMA systems. Dielectric measurements were taken on a capacity bridge of the QuadTech 1920 Precision LCR Meter for the heating cycle (QuadTech, Inc., Maynard, MA) (at measurement field frequencies from v = 0.02 kHz to 10 kHz), while magnetic properties were measured using a SQUID magnetometer (MPMS XL–7 Quantum Design, Inc., San Diego, CA) at a temperature range of −271°C to 27°C, magnetic field up to 7T, and a magnetic Faraday balance at a temperature range of 27°C–827°C. Hysteresis (P–E) loops at various electric field frequencies were investigated using a Sawyer–Tower circuit and a Matsusada (Kusatsu, Japan) HEOPS-5B6 precision high-voltage amplifier. The data were stored on a computer disk using an A/D and D/A transducer card.

Transmission Mössbauer spectra were obtained with a RENON (Cracow, Poland) MsAa-3 spectrometer, with the velocity scale calibrated by the Michelson–Morley interferometer. Spectra were collected for the 14.41 keV resonant transition in 57Fe applying a commercial 57Co (Rh) source kept together with the absorbers at room temperature. All spectra shifts are reported versus room temperature α–Fe.

The ME effect was measured at room temperature by applying a sinusoidal magnetic field H_{AC} produced by Helmholtz-type coils excited with an HD amplifier (Musial Elektronika Jądrowa, Poland) which was directed by an SR 830 lock-in amplifier (Stanford Research System, Sunnyvale, CA) and superimposed on an H_{DC} bias magnetic field produced by an electromagnet (AGH, Poland) working in tandem with a power supply (Dacpol Service, Poland).[13] The α_{ME} coefficient was calculated from the voltage output following equation (1):

$$\alpha_{ME} = \frac{V}{H_{AC} \cdot d} \tag{1}$$

where V is the voltage generated due to the magnetoelectric effect, H_{AC} is the amplitude of the sinusoidal magnetic field, and d, for both the single-phase and composite magnetoelectric media, is the thickness of the sample, as presented here.[14]

The induced voltage between sample surfaces was measured using an SR 830 lock-in amplifier working in differential mode, with an input resistance of 100 MΩ and a capacitance of 25 pF. An SM102 Hall probe system (Asonik, Tuczno, Poland) was used to measure the DC and AC magnetic fields. The composite specimens were polarized using a Matsusada Precision HEOPS-5B6 high-voltage supply. The piezoelectric parameters were determined using the resonance/antiresonance method.

Results and Discussion

Figure 1 shows X-ray spectra of synthesized PBZTMC powder at room temperature. The PBZTMC ceramics have a structure with a morphotropic area (near the rhombohedral phase). In the XRD pattern, coexistence between tetragonal (correlated with JCPDS no. 50–0346) and rhombohedral (correlated with JCPDS no. 73–2022) phases is shown. In the case of such multicomponent PZT-type solid solutions, ions of the doped elements might considerably broaden or shift the morphotropy phase boundary (MPB) toward the tetragonal or rhombohedral phase.[15] XRD patterns for the NZF ferrite powder show a typical single-phase cubic spinel.

X-ray analysis of the PBZTMC–NZF composite confirmed the presence of strong maxima originating from particular PBZTMC material phases, as well as

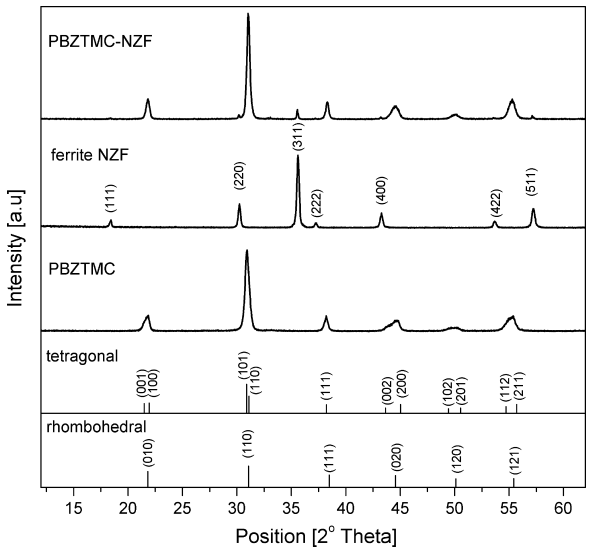

Fig. 1. Powder XRD patterns: ferroelectric PBZTMC, ferrite $Ni_{0.64}Zn_{0.36}Fe_2O_4$ (NZF) and PBZTMC–NZF composites.

weak peaks from the $Ni_{0.64}Zn_{0.36}Fe_2O_4$ ferrite, without foreign phases. Their intensity results from the percentage of the ferroelectric and ferromagnetic component in the composite.

Energy-dispersive X-ray spectroscopy was used to analyze the chemical composition of the composite samples. The EDS surface and local analyses (Fig. 2) confirmed the assumed chemical composition of the PBZTMC–NZF composite and the presence of peaks originating from the constituent ferrite and ferroelectric PBZTMC powder elements on the decay spectrum.

Figure 3 presents microstructural SEM images of fractures in the PBZTCM and NZF ceramic samples, as well as the PBZTMC–NZF composite. The microstructure of the PBZTMC ceramics (Fig. 3a) is characterized by small, well-crystallized grains. Such a proper microstructure is guaranteed by the optimum technological conditions of the ceramics preparation, as well as its multi-component chemical composition. Cations of the manganese additive give order to the microstructure (increasing the homogeneity of the grains), whereas the

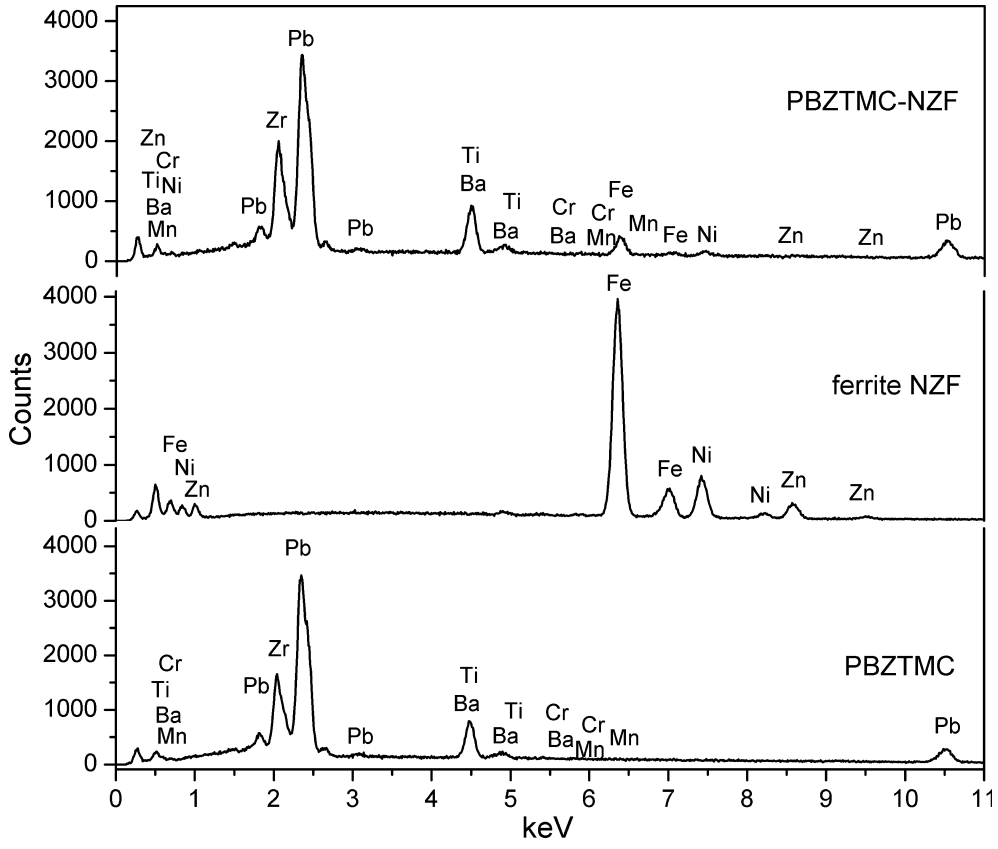

Fig. 2. The distribution of elements (energy-dispersive X-ray spectroscopy [EDS]) for PBZTMC ceramics, ferrite (NZF), and PBZTMC–NZF composite.

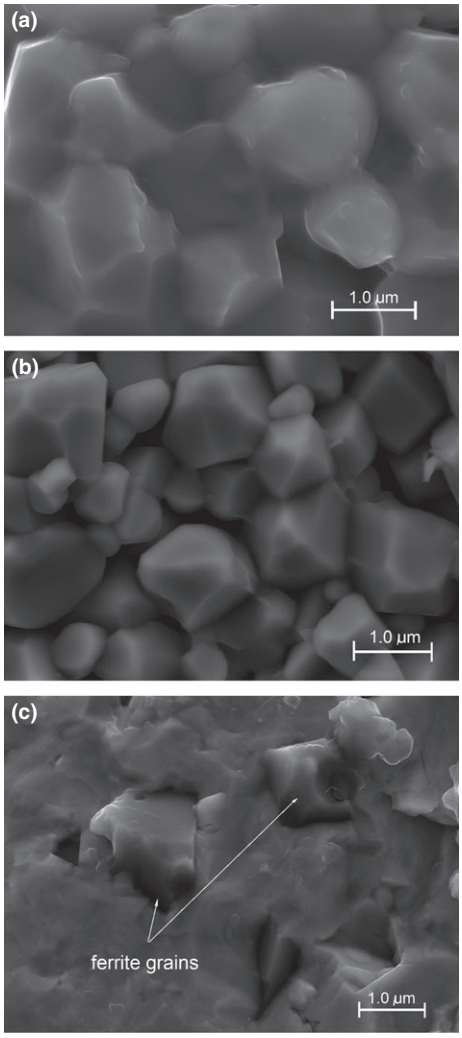

Fig. 3. SEM microstructures: (a) PBZTMC ceramics, (b) ferrite NZF sample, and (c) PBZTMC–NZF composite.

additive of chromium impedes excessive grain growth in the solid solution.[10] Some of the cations of the chromium additive which do not dissolve in the lattice accumulate on the grain boundaries, restraining their growth. The limiting layer between the grains is not unequivocally glasslike; however, it differs from the crystallite-creating grains in terms of interference density, amount of energy, chemical and phase composition, etc., which results in differences of conductivity and electric permittivity of the limiting layer and the interior of the grain, among other things.

The microstructure of the ferrite ceramics sample shows a characteristic cubic grain shape (Fig. 3b), while the SEM microstructure of the PBZTMC–NZF composite shows heterogeneity. High-temperature sintering

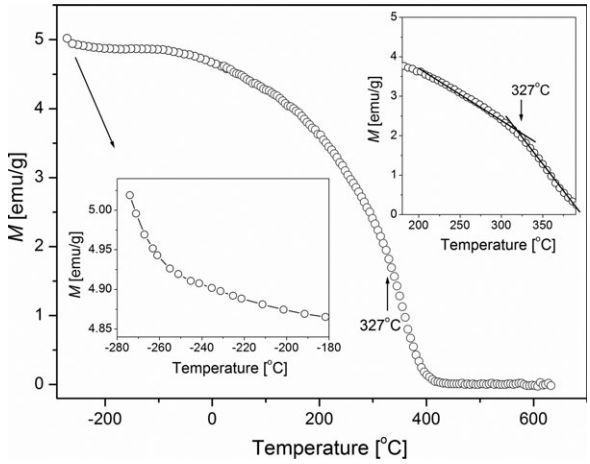

Fig. 4. Magnetization temperature dependencies for PBZTMC–NZF composite.

causes the grains and intergranular phase of the ferroelectric component of the composite to strongly solidify (no well-developed grains with boundaries of the ferroelectric component were observed — Fig. 3c). In the microstructure of the fracture of the ferroelectric–ferromagnetic composites, PBZTMC–NZF shows that the ferrite grains on the surface of the ferroelectric component are distributed heterogeneously. Ferrite grains are usually tetrahedral in shape (marked in Fig. 3c).

At the same time, the EPMA analysis of element distribution homogeneity with an X-ray probe revealed a minor presence of iron in the area of the ferroelectric grains on the surface of the composite samples' microstructure fracture (not presented in this work).

The temperature dependence of the magnetization $M(T)$ of the PBZTMC–NZF composite (Fig. 4) consists of two components, namely the ferro/ferrimagnetism with a Curie temperature of nearly 410°C and the para-/super-paramagnetic visible at temperatures under −180°C (left side of the Fig. 4 –inside).

The character of $M(T)$ indicates the presence of large grains with domains of ferromagnetic order, as well as smaller (noninteracting) grains exhibiting para-/superparamagnetic properties in the sample. At the temperature of approx. 327°C, in the PBZTMC–NZF composite of ferroelectric–paraelectric phase transition zone, there exists an inflexion in the form of a change of slope of the $M(T)$ (see the right side of Fig. 4 – inside). This particular behavior may indicate that the electric subsystem influences the PBZTMC–NZF magnetic properties.

The behavior of the magnetic hysteresis loop $M(H)$ of the PBZTMC–NZF composite (in the temperatures of −271°C, −173°C, and 27°C) is characteristic of soft

ferromagnetic materials (Fig. 5). Coercivity (the highest for 27°C) and nonzero remanence magnetization appear on the $M(H)$ loops. The coercivity values are $\mu_0 H_C = 0.13$ T for −271°C, $\mu_0 H_C = 0.11$ T for −171°C, and $\mu_0 H_C = 0.15$ T for 27°C. This behavior can be attributed to the ferrimagnetic structure of magnetic moments in the PBZTMC–NZF composites. Together with an increase in temperature, the remanence magnetization ($M_r = 2.70$ emu/g for −271°C, $M_r = 2.45$ emu/g for −171°C, and $M_r = 1.71$ emu/g for 27°C) and spontaneous magnetization ($M_S = 6.52$ emu/g for −271°C, $M_S = 5.90$ emu/g for −171°C, and $M_S = 3.47$ emu/g for 27°C) decrease.

Mössbauer investigations of the PBZTMC–NZF composite performed at room temperature in transmission geometry (Fig. 6 and Table I) indicate the presence of three absorption cross-sections originating from the ferrite (NZF), PBZTMC phase, and some additional component due to a minor impurity phase. The magnetically split spectral component is generated by the Fe^{3+} high spin ion. This ion is located in the ferrite and has high crystallographic local symmetry, as the electric quadrupole interaction is negligible. A spectral doublet originates from the paramagnetic PBZTMC phase with lower symmetry around iron, which causing quadrupole splitting to occur. The ionic state of iron is Fe^{3+} with high spin at this site. The PBZTMC compound does not include iron atoms prior to the synthesis of the composite. The Mössbauer result indicates that after synthesis of the composite PBZTMC–NZF, the iron distribution is 79 at-% in NZF (Fe^{3+}) and 17 at-% in PBZTMC (Fe^{3+}). Hence, the Fe^{3+} iron is transferred from the ferrite to the PBZTMC phase during annealing.

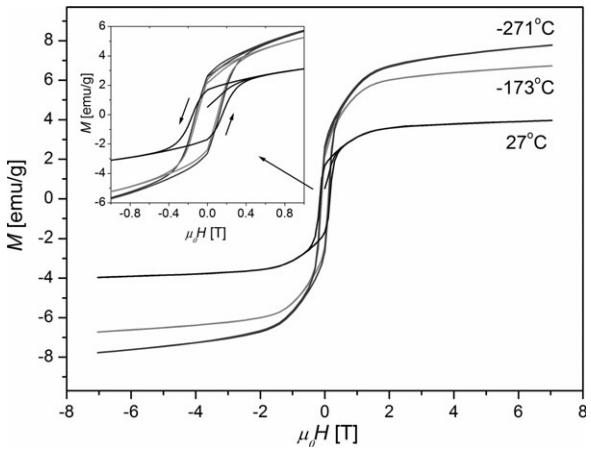

Fig. 5. Magnetic hysteresis loop for PBZTMC–NZF composite.

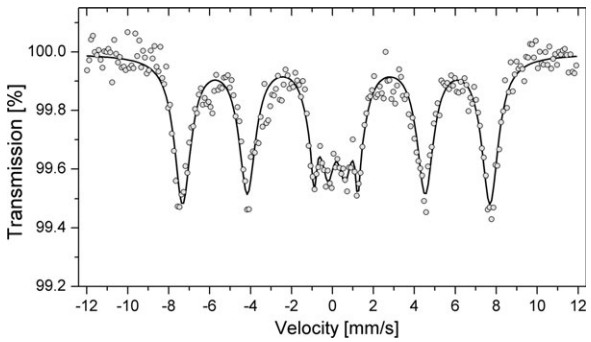

Fig. 6. ^{57}Fe Mössbauer spectra for PBZTMC–NZF composite.

Table I. The Values of Hyperfine Parameters (*IS*, *QS*, B_{hf}) and *A* for Composite PBZTMC–NZF, Where *A* is the Contribution of the Respective Sub-profile (phase/iron Site) to the Total Absorption Profile; *IS* is Isomeric Shift; *QS* is Quadrupole Splitting; and B_{hf} is Hyperfine Magnetic Field. Errors for all Values are of the Order of Unity for the last Digit Shown

	A [%]	*IS* [mm/s]	*QS* [mm/s]	B_{hf} [*T*]
NZF	79	0.3	–	46.5
PBZTMC	17	0.3	0.8	–
Impurity phase	4	0.3	2.2	–

The temperature changes of electric permittivity (ε) and the tangent of the angle of dielectric loss (tan δ) for the PBZTMC ceramics are typical for the multicomponent PZT-type family of ceramics (Figs. 7a and 8a).[16] The PBZTMC ceramics have a sharp phase transition with high values of maximum electric permittivity. At the same time, dispersion of the resonance frequency on the ε (T) graphs is not observed. In the case of the PBZTMC–NZF composite, the Curie temperature may be seen to decrease on the ε (T) graphs (Fig. 7b). Introducing a magnetic component to the PBZTMC also causes the maximum value of electric permittivity to decrease (particularly visible for higher frequencies of the measurement field). On the PBZTMC–NZF composite ε (T) graphs, high ferroelectric phase transition broadening is observed, with a small Curie temperature shift toward lower temperatures and with an increase in the measurement field. This particular behavior might be attributable to the magnetic subsystem ($Ni_{0.64}Zn_{0.36}Fe_2O_4$ ferrite) phase transition temperatures overlapping, as well as to the PBZTMC material electric subsystem. It may also indicate the influence of the magnetic subsystem on the PBZTMC–NZF composite electric properties.

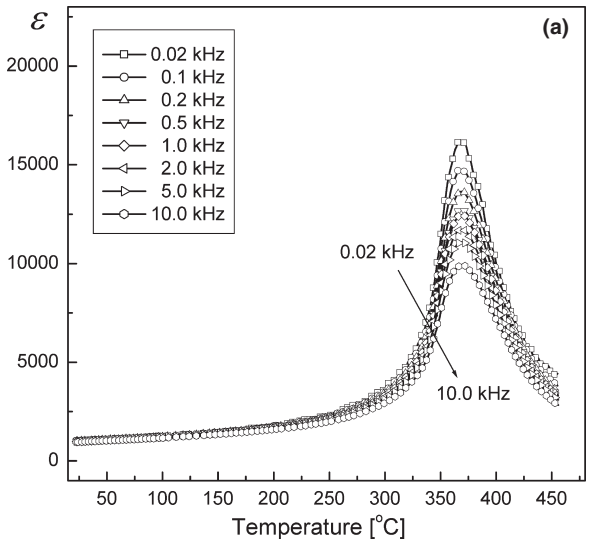

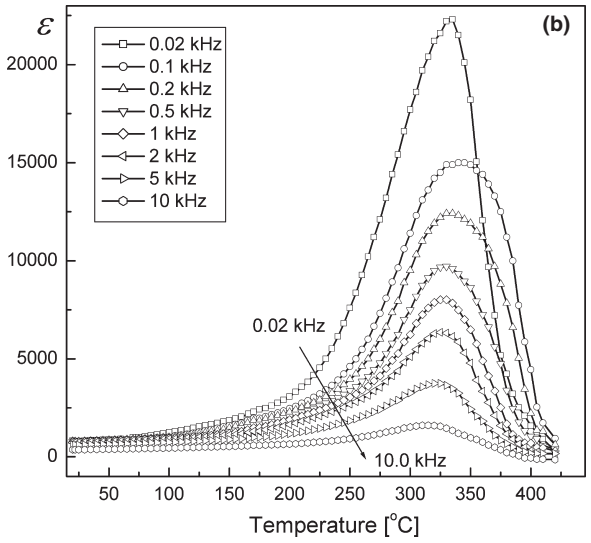

Fig. 7. Temperature dependencies of electric permittivity ε for (a) PBZTMC ceramics and (b) PBZTMC–NZF composite (heating).

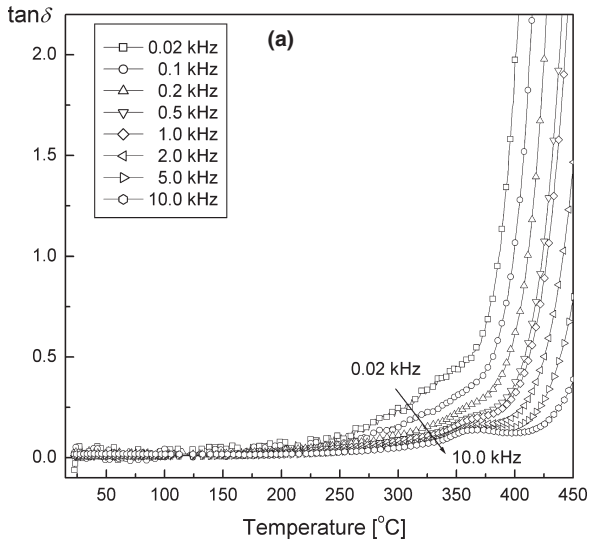

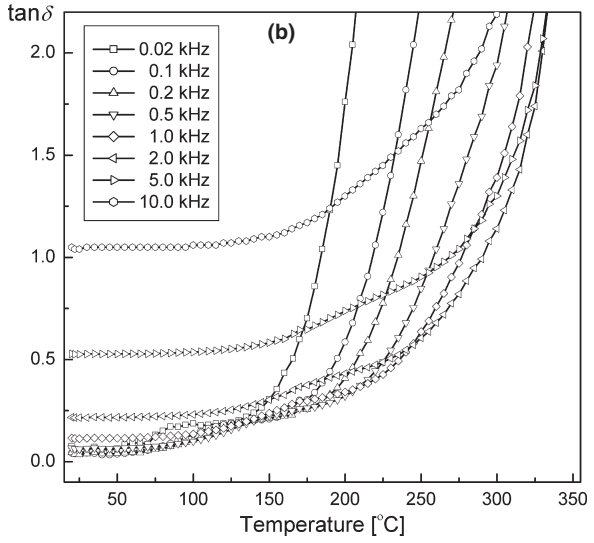

Fig. 8. Temperature dependencies for tangent of dielectric losses tan δ for (a) PBZTMC ceramics and (b) PBZTMC–NZF composite (heating).

In the two-phase PBZTMC–NZF ceramic composite, the magnetic component also causes the dielectric loss to increase in comparison with the PBZTMC ceramics (Fig. 8). A rapid increase (related to a significant increase of electric conductivity) occurs above 150°C. This is due to a much lower ferrite resistance as compared to the PBZTMC ferroelectric material, which decreases significantly as the temperature increases.

Figure 9 shows an electric hysteresis loop for the PBZTMC ceramics and the PBZTMC–NZF composite obtained at room temperature. The PBZTMC ceramics have an electric hysteresis loop characteristic for linear dielectrics with losses (P_R = 2.24 μC/cm^2, E_C = 0.63 kV/mm). The electric hysteresis loops of the PBZTMC–NZF ceramics have a shape typical of the linear dielectrics with losses, but have slightly lower residual polarization (P_R) and a much higher coercive field E_C (E_C increases as the measurement field frequency decreases).

Samples of the PBZTMC ceramics and the PBZTMC–NZF ceramic composite underwent a high-voltage poling process (in silicone oil). For the PBZTMC ceramics, it was possible to apply a high E_{pol} poling field and to increase the t_{pol} poling time and the poling temperature (limited by the working temperature

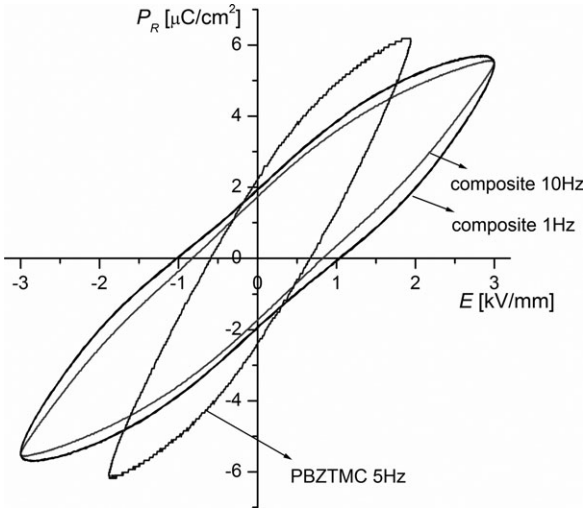

Fig. 9. Electric hysteresis loops for PBZTMC–NZF composite and PBZTMC ceramics.

Table II. Parameters of the PBZTMC Ceramics and PBZTMC–NZF Composite (Dielectric Properties for ν = 1 kHz)

	PBZTMC	PBZTMC–NZF
ρ [g/cm^3]	7.6	6.9
T_m [°C]	370	327
ε_r	1020	850
ε_m	12,430	7990
tan δ at T_r	0.01	0.11
tan δ at T_m	0.20	2.40
k_p	0.59	0.31
$d_{31} \times 10^{-12}$ [C/N]	119.84	20.53
$S_{11}^E \times 10^{-12}[m^2/N]$	1.432	0.78
$g_{31} \times 10^{-3}$ [Vm/N]	12.25	3.44

of the silicone oil). The PBZTMC poling conditions were E_{pol} = 40 kV/cm, t_{pol} = 0.5 h, T_{pol} = 160°C. However, because of a breakdown possibility of the PBZTMC–NZF composite sample caused by higher electric conductivity, the conditions were changed to T_{pol} = 80°C, E_{pol} = 25 kV/cm, t_{pol} = 3 h. The piezoelectric parameters of the polarized samples are presented in Table II.

Figure 10a shows the relations of magnetoelectric coefficient α_{ME} with a constant H_{DC} magnetic field measured at H_{AC} = 5 Oe and ν = 1 kHz. For Fig. 10b, the relations of magnetoelectric coefficient α_{ME} with the measurement field frequency ν were measured with H_{DC} = 1200 Oe and H_{AC} = 5 Oe. High piezoelectric

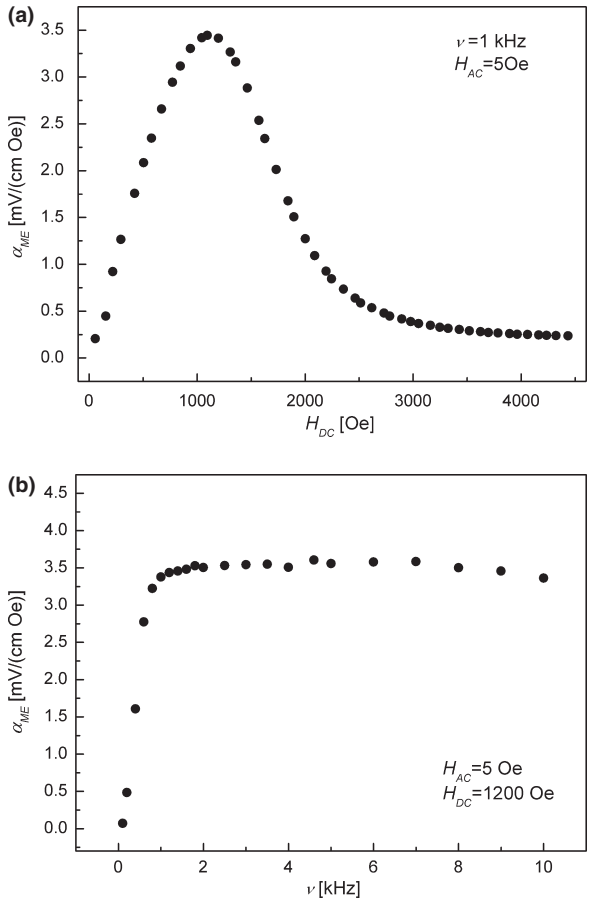

Fig. 10. The magnetoelectric coefficient α_{ME} for PBZTMC–NZF composite as a function (a) of bias magnetic field H_{DC} and (b) of frequency ν.

parameter values of the PBZTMC ceramics decrease significantly when combined with the ferrite to form the PBZTMC–NZF composite. What is more, the PBZTMC–NZF composite, in comparison with the PZT-type ceramics, is more difficult to polarize.

In Fig. 10a, the magnetoelectric coefficient, α_{ME},[17] determined for PBZTMC–NZF composite is plotted versus the bias magnetic field H_{DC}. The AC and DC magnetic fields were applied perpendicularly to the sample surfaces. With a lower magnetic field, the α_{ME} coefficient strongly increases before reaching its maximum at H_{DC} = 1100 Oe and then decreasing. The dependence α_{ME} vs. H_{DC} is possibly due to the piezomagnetic coefficient $d\lambda/dH$, where λ is the magnetostriction.

For the PBZTMC–NZF composite, the α_{ME} values strongly increase with frequencies changing from 10 Hz to 1 kHz and reach an almost constant maximum level in the range of 1–10 kHz. In general, magnetoelectric coupling between the magnetostrictive phase and the fer-

roelectric phase increases with the frequency of the AC magnetic field rising up to a value corresponding to the resonance magnetoelectric effect and then decreases.[18] However, the frequency dependencies of the magnetoelectric coefficient obtained using measurement or theoretical calculations for magnetoelectric composites by other authors are similar to our dependencies.[19,20] They suggest that the magnetoelectric coefficient in the low frequency region depends on the composition of the composite and conductivity of the ferrite phase.

Conclusions

In the work, a ceramic composite PBZTMC–NZF consisting of the $(Pb_{0.94}Ba_{0.06})(Zr_{0.52}Ti_{0.48})O_3$ + 0.1wt-% MnO_2 + 0.15wt-% Cr_2O_3 (PBZTMC) ferroelectric powder and ferrite $Ni_{0.64}Zn_{0.36}Fe_2O_4$ (NZF) powder was designed and successfully obtained. The study presented the effect of combining ferroelectric and ferromagnetic material in the form of composite PBZTMC–NZF on the microstructure and the basic dielectric and magnetic properties.

X-ray analysis of the two-phase PBZTMC–NZF ceramic composite confirmed the presence of phases originating from the ferroelectric and magnetic component (without foreign phases), while the SEM analysis confirmed the composite character of the material's microstructure (smaller ferrite grains surrounded by the larger grains of the PBZTMC ferroelectric component).

Very good ferroelectric and piezoelectric properties of the multicomponent PBZTMC solid solution and strong ferromagnetic properties of the ferrite NZF make it possible to obtain multiferroic composites of various applications. Magnetic researches have shown that a content of 10 wt-% ferrite is a substantial amount to maintain its good ferromagnetic properties in the PBZTMC–NZF composite, ensuring the maintenance of high dielectric properties.

To increase the potential use of this type of material, the proportions of the ferroelectric and ferromagnetic component in the PBZTMC–NZF composite (the magnetic properties can be improved by increasing the amount of ferrite to 30%) can be changed. Such a change, however, entails reducing the ferroelectric properties of the composite.

The coexistence of ferroelectric and ferromagnetic properties of PBZTMC–NZF composites may be used in constructing magnetoelectric transducers or new types of memory.

Acknowledgments

We are grateful for the assistance of Anna Łatkiewicz (Laboratory of FE Scanning Microscopy and Microanalysis, Institute of Geological Sciences, Jagiellonian University, Cracow, Poland) for her help with the SEM pictures and XRD measurements.

References

1. J. F. Scott, *J. Mater. Chem.*, 22 4567–4574 (2012).
2. D. Khomskii, *Physics*, 2 [20], (2009) doi: 10.1103/Physics.2.20.
3. H. Schmid, *J. Phys.: Condens. Matter*, 20, 434201–434201-24 (2008).
4. C.-W. Nan, M. I. Bichurin, S. Dong, D. Viehland, and G. Srinivasan, *J. Appl. Phys.*, 103, 031101–031101-35 (2008).
5. D. Bochenek, P. Niemiec, P. Wawrzała, and A. Chrobak, *Ferroelectrics*, 448 96–105 (2013).
6. D. Bochenek, P. Niemiec, A. Chrobak, G. Ziółkowski, and A. Błachowski, *Mater. Charact.*, 87 36–44 (2014).
7. J. Bartkowska and J. Ilczuk, *Acta Phys. Pol., A*, 114 A7–A13 (2008).
8. P. Guzdek, M. Sikora, Ł. Góra, and Cz. Kapusta, *J. Eur. Ceram. Soc.*, 32 2007–2011 (2012).
9. Z. Surowiak and D. Bochenek, *Arch. Acoust.*, 33 243–260 (2008).
10. D. Bochenek and Z. Surowiak, *Phys. Status Solidi A*, 206 2857–2865 (2009).
11. S. B. Majumder, S. Bhattacharyya, R. S. Katiyar, A. Manivannan, P. Dutta, and M. S. Seehra, *J. Appl. Phys.*, 99, 024108-1–024108-9 (2006).
12. L. Kozielski and M. Adamczyk, *Arch. Metall. Mater.*, 56 1111–1117 (2011).
13. D. Bochenek and P. Guzdek, *J. Magn. Magn. Mater.*, 323 369–374 (2011).
14. M. Fiebig, *J. Phys. D: Appl. Phys.*, 38 R123–R152 (2005).
15. E. Boucher, B. Guiffard, L. Lebrun, and D. Guyomar, *Ceram. Int.*, 32 479–485 (2006).
16. R. Zachariasz and D. Bochenek, *Arch. Metall. Mater.*, 54, 895–902 (2009).
17. V. B. Naik and R. Mahendiran, *Solid State Commun.*, 149 754–758 (2009).
18. A. Kumar, R. S. Katiyar, and J. F. Scott, *J. Appl. Phys.*, 108, 064105-1–064105-10 (2010).
19. Y. K. Fetisov, K. E. Kamentsev, and A. Y. Ostashchenko, *J. Magn. Magn. Mater.*, 272–276, 2064–2066 (2004).
20. V. M. Petrov, M. I. Bichurin, G. Srinivasan, J. Zhai, and D. Viehland, *Solid State Commun.*, 142 515–518 (2007).